IJCFD, 1997, Vol. 9, pp. 1–22
Reprints available directly from the publisher
Photocopying permitted by license only

A Finite Volume Extension of the Lax-Friedrichs and Nessyahu-Tadmor Schemes for Conservation Laws on Unstructured Grids

P. ARMINJON[a], M.-C. VIALLON[b] and A. MADRANE[a]

[a]*Dép. de mathématiques et de statistique, Université de Montréal*
C.P. 6128, Succ. centre-ville, Montréal, Québec, Canada, H3C 3J7;
[b]*Équipe d'analyse numérique, Université de Saint-Étienne, 23 rue Paul Michelon,*
42023 Saint-Étienne Cedex 2, France

(Received 7 July 1996; In final form 2 December 1996)

The non-oscillatory central difference scheme of Nessyahu and Tadmor, in which the resolution of Riemann problems at the cell interfaces is by-passed thanks to the use of the staggered Lax-Friedrichs scheme, is extended here to a two-step, two-dimensional non-oscillatory centered scheme in finite volume formulation. The construction of the scheme rests on a finite volume extension of the Lax-Friedrichs scheme, in which the finite volume cells are the barycentric cells constructed around the nodes of an FEM triangulation, for odd time steps, and some quadrilateral cells associated with this triangulation, for even time steps.

Piecewise linear cell interpolants using least-squares gradients combined with a van Leer-type slope limiting allow for an oscillation-free second-order resolution.

Some preliminary numerical experiments suggest that two-dimensional problems can be handled very efficiently by the method presented here.

Keywords: Hyperbolic conservation laws, finite volumes, unstructured staggered grids, MUSCL interpolants, slope limiters, compressible flows

1. INTRODUCTION

In an attempt to construct a simplified version of high resolution non-oscillatory Godunov-type methods for the numerical approximation of hyperbolic conservation laws [17], Nessyahu and Tadmor [13] recently proposed, for one-dimensional problems, an elegant difference scheme based on a combination of the staggered form of the Lax-Friedrichs scheme [20] and the use of van Leer's MUSCL piecewise linear interpolants [11], [12] in a Godunov-type approach, decomposed in two steps for second-order time and space accuracy.

The main feature of their scheme lies in the fact that it does not require the detailed exact or approximate solution of the local Riemann problems ([10], [14], [15], [16]) generated at the cell interfaces, thanks to the use of the staggered form of the Lax-Friedrichs scheme. Since the scheme proposed by Nessyahu and Tadmor was constructed for one space dimension, we shall present in this paper a two-dimensional method, based on the principle of their scheme, in a finite volume formulation, along the lines of some earlier work ([1], [4], [5]).

In [21], we had described an extension of the Lax-Friedrichs and Nessyahu-Tadmor schemes to two-dimensional rectangular grids. In this paper, we present our two-dimensional extension to unstructured triangular grids (see also [3] for other numerical experiments than those presented here).

In other papers, ([6], [18], [19]), we study the convergence of our method for scalar two-dimensional conservation laws, and prove a maximum principle and a result on the L^∞-*weak** convergence of the numerical solution to a weak solution of the scalar equation $u_t + \mathrm{div}(u\vec{V}) = 0$ with $\mathrm{div}\,\vec{V} = 0$.

In section 2, we give a short description of the Nessyahu-Tadmor (NT) scheme; section 3 presents a two-dimensional finite-volume extension of the Lax-Friedrichs scheme using the barycentric cells constructed around the nodes of an arbitrary (unstructured) triangular Finite Element grid and a dual set of quadrilateral cells; we then present in section 4 a two-dimensional finite volume scheme for arbitrary triangular grids which is inspired, in its construction, by our Finite Volume Lax-Friedrichs scheme and the Nessyahu-Tadmor difference scheme. Some early numerical experiments are then presented in section 5 (Linear advection, Supersonic Euler flow around a NACA 0012 airfoil, Supersonic flow around a double ellipse).

2. DESCRIPTION OF THE 1-DIMENSIONAL NESSYAHU-TADMOR SCHEME

To approximate the solution of the scalar conservation law

$$u_t + f(u)_x = 0 \qquad (2.1)$$

$$-\infty < x < \infty$$

with initial condition

$$u(x,0) = u_0(x) \qquad (2.1')$$

we first consider Godunov's [10] approximate solution $\bar{u}(x,t^n)$, which is piecewise constant on the cells $C_j = (x_{j-1/2}, x_{j+1/2})$, for $t = t^1, \ldots, t^n, \ldots$ (with $t^0 = 0$):

$$\bar{u}(x,t^n) = \bar{u}_j^n \qquad (2.2)$$

(defined below) for $x_{j-1/2} < x < x_{j+1/2}$.

Starting from the piecewise constant initial approximation

$$\bar{u}^0(x,0) = \bar{u}_j^0 = \frac{1}{\Delta x}\int_{x_{j-1/2}}^{x_{j+1/2}} u_0(x)\,dx \qquad (2.3)$$

for $x_{j-1/2} < x < x_{j+1/2}$,

Godunov's method evolves this initial function for a time $\Delta t = t^1 - t^0$ small enough to prevent the corresponding Riemann problems generated at the cell interfaces $x_{j+1/2}$ to interact with each other, thus defining an approximate solution

$$v(x,t^1) = R\left(\frac{x - x_{j+1/2}}{\Delta t}; \bar{u}_j^0, \bar{u}_{j+1}^0\right) \quad x_j < x < x_{j+1} \qquad (2.4)$$

where $R(x/t, u_l, u_r)$ is the self-similar exact solution of the Riemann problem for (2.1) at $x_0 = 0, t \geqslant t^0 = 0$ with

$$u(x,0) = \begin{cases} u_l & x < 0 \\ u_r & x > 0. \end{cases}$$

The new cell values $\bar{u}_j^1$ are then defined by the cell averages of $v(x,t^1)$:

$$\bar{u}_j^1 = \frac{1}{\Delta x}\int_{C_j} v(x,t^1)\,dx =$$

$$= \frac{1}{\Delta x}\left\{\int_{x_{j-1/2}}^{x_j} R\left(\frac{x - x_{j-1/2}}{\Delta t}; \bar{u}_{j-1}^0, \bar{u}_j^0\right) dx \right.$$

$$\left. + \int_{x_j}^{x_{j+1/2}} R\left(\frac{x - x_{j+1/2}}{\Delta t}; \bar{u}_j^0, \bar{u}_{j+1}^0\right) dx \right\} \quad (2.5)$$

The typical time step $t^n \to t^{n+1}$ follows the same pattern, and can be written in conservation form:

$$\bar{u}_j^{n+1} = \bar{u}_j^n - \lambda[f(R(o^+; \bar{u}_j^n, \bar{u}_{j+1}^n))$$

$$- f(R(o^+; \bar{u}_{j-1}^n, \bar{u}_j^n))] \quad \left(\lambda \equiv \frac{\Delta t}{\Delta x}\right). \quad (2.6)$$

Since our aim is to solve systems of conservation laws, (2.6) shows that Godunov's method requires the detailed (exact or approximate) solution of the Riemann problems posed at the cell interfaces, a time-consuming task which the Nessyahu-Tadmor schemes by-passes thanks to a judicious use of the Lax-Friedrichs scheme [20], written in its staggered form as

$$u_{j+1/2}^{n+1} = \frac{1}{2}(u_j^n + u_{j+1}^n) - \lambda[f(u_{j+1}^n) - f(u_j^n)] \quad (2.7)$$

which can also be interpreted as an application of Godunov's scheme over the staggered grid corresponding to the cells $C_{j+1/2} = (x_j, x_{j+1})$:

$$u_{j+1/2}^{n+1} = \frac{1}{\Delta x}\int_{x_j}^{x_{j+1}} R\left(\frac{x - x_{j+1/2}}{\Delta t^{n+1} - t^n}; u_j^n, u_{j+1}^n\right) dx \quad (2.8)$$

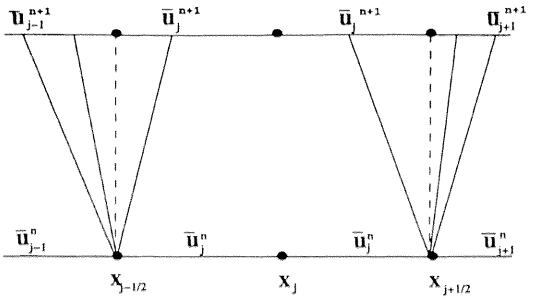

FIGURE 1 Non-interacting Riemann problems at the cell endpoints.

starting from cell values $\{u_j^n\}$ defined on the cells $\{(x_{j-1/2}, x_{j+1/2})\}$ of the original grid; the integral in the R.H.S. is computed by integrating (2.1) on $[x_j, x_{j+1}] \times [t^n, t^{n+1}]$ with the help of Green's formula. To complete a computation cycle, and come back to the original gridpoints $\{x_j\}$, we must then perform a second step with the help of the staggered gridpoints:

$$u_j^{n+2} = \frac{1}{2}(u_{j-1/2}^{n+1} + u_{j+1/2}^{n+1})$$

$$- \lambda[f(u_{j+1/2}^{n+1}) - f(u_{j-1/2}^{n+1})]. \quad (2.7')$$

To reduce the numerical dissipation of the scheme and obtain second order accuracy, the Nessyahu-Tadmor scheme then replaces Godunov's piecewise constant cell values by piecewise linear MUSCL-type interpolants: at the beginning of each time step, we first reconstruct, from the piecewise constant cell average approximation (2.2) obtained at the end of the previous time step, a piecewise linear approximation of the form

$$L_j(x, t^n) = \bar{u}_j^n + (x - x_j)\frac{\delta_j^n}{\Delta x} \quad x_{j-1/2} < x < x_{j+1/2}. \quad (2.9)$$

In this way, conservation is retained

$$\overline{L_j}(t^n) \equiv \frac{1}{\Delta x}\int_{x_{j-1/2}}^{x_{j+1/2}} L_j(x, t^n) = \bar{u}_j^n \quad (2.9')$$

and it can be shown ([13]) that second order accuracy is obtained if the numerical derivative $\delta_j^n/\Delta x$ (to be defined below) satisfies

$$\frac{\delta_j^n}{\Delta x} = \frac{\partial}{\partial x} u(x, t^n)\bigg|_{x = x_j} + O(\Delta x). \quad (2.9'')$$

The piecewise linear interpolants (2.9) are then advanced in time by considering the (exact) solution of the non-interacting generalized Riemann

problems thus defined at the cell interfaces $x_{j+1/2}$

$$v(x,t^{n+1}) = GR(x,t^{n+1};L_j(x,t^n),$$

$$L_{j+1}(x,t^n)) \quad x_j < x < x_{j+1} \tag{2.10}$$

from which the new staggered cell average values $\bar{u}^{n+1}_{j+1/2}$ at time t^{n+1} are now defined as

$$\bar{u}^{n+1}_{j+1/2} = \frac{1}{\Delta x}\int_{x_j}^{x_{j+1}} v(x,t^{n+1})dx \tag{2.11}$$

representing the Nessyahu-Tadmor numerical approximation for $x_j < x < x_{j+1}$.

This integral can be computed without actually solving the generalized Riemann problems by first integrating the conservation law (2.1) on the rectangle $\mathscr{R}^n_{j+1/2} \equiv (x_j, x_{j+1}) \times (t^n, t^{n+1})$ to obtain, with Green's theorem (Fig. 2):

$$\oint_{\partial \mathscr{R}^n_{j+1/2}} (u\,dx - f(u)dt) = 0. \tag{2.12}$$

Applying (2.12) to the function $v(x,t) = GR(x,t; L_j(x,t^n), L_{j+1}(x,t^n))$ then leads to

$$\Delta x \cdot \bar{u}^{n+1}_{j+1/2} = \int_{x_j}^{x_{j+1/2}} L_j(x,t^n)dt$$

$$+ \int_{x_{j+1/2}}^{x_{j+1}} L_{j+1}(x,t^n)$$

$$- \int_{t^n}^{t^{n+1}} f(v(x_{j+1},t))dt$$

$$+ \int_{t^n}^{t^{n+1}} f(v(x_j,t))dt. \tag{2.13}$$

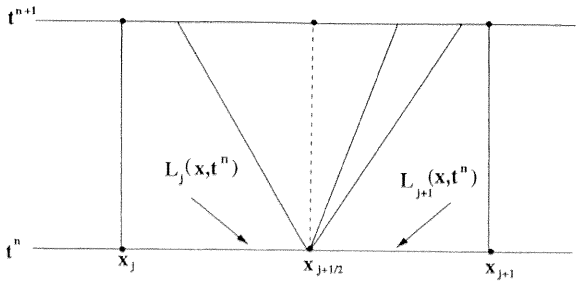

FIGURE 2 Line integral on $\partial \mathscr{R}^n_{j+1/2}$.

In the last two integrals, the integrands are smooth functions of t under the CFL condition

$$\lambda \cdot \max_{x_j \leqslant x \leqslant x_{j+1}} \rho(A(v(x,t))) < \frac{1}{2} \tag{2.14}$$

where $\rho(A)$ is the spectral radius of $A(v) \equiv f'(v)$ if (2.1) is a system, and $\rho(A) \equiv |f'(v)|$ if (2.1) is a scalar conservation law. Using (2.9) we can compute the first two integrals exactly, and applying the midpoint rule (with an $O[(\Delta t)^3]$error) to the flux integrals, we get the numerical approximation

$$\bar{u}^{n+1}_{j+1/2} = \frac{1}{2}(\bar{u}^n_j + \bar{u}^n_{j+1}) + \frac{1}{8}(\delta^n_j - \delta^n_{j+1})$$

$$- \lambda[\, f(v(x_{j+1}, t^{n+1/2}))$$

$$- f(v(x_j, t^{n+1/2}))] \tag{2.15}$$

where $t^{n+1/2} = t^n + \Delta t/2$,

In [13] the values of $v(x_j, t^{n+1/2})$ needed in (2.15) are approximated as

$$v(x_j, t^{n+1/2}) \cong v(x_j, t^n) + \frac{\Delta t}{2} v_t(x_j, t^n)$$

$$\cong \bar{u}^n_j - \frac{\Delta t}{2} \cdot \frac{f'_j}{\Delta x} \equiv u^{n+1/2}_j \tag{2.16a}$$

where $(1/\Delta x) f'_j$ stands for an approximate numerical derivative of the flux $f(v(x,t))$:

$$\frac{1}{\Delta x} f'_j = \frac{\partial}{\partial x} f(v(x,t^n))\bigg|_{x=x_j} + O(\Delta x) \tag{2.17}$$

for which several possibilities are studied in [13].

Observe that we could also choose to use (2.9″) in $f(v)_x = f'(v)v_x$ and consider instead of (2.16) the

following approximation

$$v(x_j, t^{n+1/2}) \cong \bar{u}_j^n - \frac{\Delta t}{2} f'(\bar{u}_j^n) \frac{\delta_j^n}{\Delta x} \equiv \tilde{u}_j^{n+1/2}. \quad (2.16b)$$

Whatever our choice for the intermediate value, $u_j^{n+1/2}$ or $\tilde{u}_j^{n+1/2}$, the NT scheme can be considered as a predictor (2.16) followed by a corrector (2.15).

To retrieve the original grid $\{x_j\}$ we then perform the alternate time step

$$\bar{u}_j^{n+2} = \frac{1}{2}(\bar{u}_{j+1/2}^{n+1} + \bar{u}_{j-1/2}^{n+1}) + \frac{1}{8}(\delta_{j-1/2}^{n+1} - \delta_{j+1/2}^{n+1}) - \lambda[f(u_{j+1/2}^{n+3/2}) - f(u_{j-1/2}^{n+3/2})]$$

where the definitions of $\delta_{j+1/2}^{n+1}, u_{j+1/2}^{n+3/2}$ are similar to (2.9″) and (2.16a)–(2.16b), respectively. One of the approximations considered in [13] for δ_j^n(written as v_j' there) is

$$\delta_j^n = MM\left\{\alpha\Delta\bar{u}_{j+1/2}^n, \frac{1}{2}(\bar{u}_{j+1}^n - \bar{u}_{j-1}^n), \alpha\Delta\bar{u}_{j-1/2}^n\right\}$$

$$\equiv \min \text{ mod}\left\{\alpha(\bar{u}_{j+1}^n - \bar{u}_j^n), \frac{1}{2}(\bar{u}_{j+1}^n - \bar{u}_{j-1}^n), \alpha(\bar{u}_j^n - \bar{u}_{j-1}^n)\right\} \quad (2.18)$$

where $\alpha \in [0, 4]$ is a parameter discussed in [13].

Under appropriate conditions, the NT scheme is then shown to be second-order accurate and TVD (see [13]).

3. TWO-DIMENSIONAL FINITE VOLUME EXTENSION OF THE LAX-FRIEDRICHS SCHEME

We consider the solution $u(x, y, t)$ of the two-dimensional scalar conservation equation

$$u_t + f(u)_x + g(u)_y = 0 \quad (3.1)$$

in some region Ω of the $x - y$ plane. In one space dimension, we have seen that both the staggered form of the Lax-Friedrichs scheme and the Nessyahu-Tadmor scheme use two alternate grids $\{x_j\}$ and $\{x_{j+1/2}\}$ at odd and even time steps, respectively. In two dimensions, we proceed in a similar way, starting from an arbitrary FEM triangular grid $\mathcal{T}_h$ such that

$$\Omega = \bigcup_{T \in \mathcal{T}_h} T \text{ and } T \cap T' = \begin{cases} \phi \\ \text{one vertex} \\ \text{one side} \end{cases} \text{ for any } T, T' \in \mathcal{T}_h \quad (3.2)$$

The nodes of the FEM triangulation are the vertices a_i of the triangles, and the degrees of freedom are the values of u at the nodes, which can also be considered as cell average values for the cell C_i centered at each individual node a_i (defined below).

For the first grid associated with our finite volume extension of the Lax-Friedrichs scheme, the nodes are the vertices a_i of $\mathcal{T}_h$ while the finite volume cells are the barycentric cells C_i associated with these nodes, obtained by joining the midpoints M_{ij} of the sides originating in a_i to the centroids G_{ij} of the triangles of $\mathcal{T}_h$ which meet at a_i (Fig. 3).

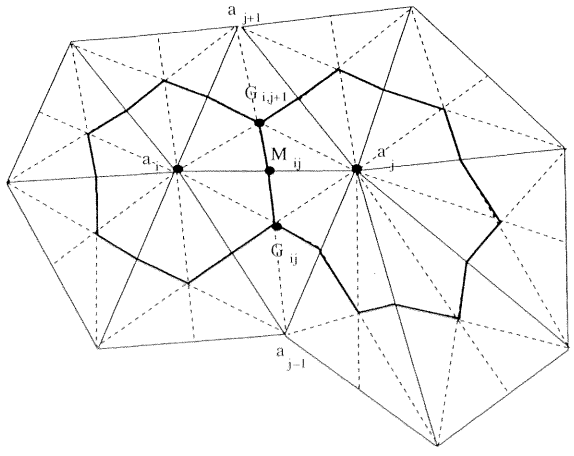

FIGURE 3 Barycentric cells around nodes a_i, a_j; quadrilateral cell $a_i G_{ij} a_j G_{i,j+1}$.

For the second grid the nodes are the midpoints M_{ij} of the sides of the original triangulation, while the cells are the quadrilaterals of the form $L_{ij} = a_i G_{ij} a_j G_{i,j+1}$ having M_{ij} as midpoint of one diagonal, obtained by joining two adjacent nodes a_i, a_j to the centroids of the two triangles of $\mathcal{T}_h$ of which $a_i a_j$ is a side.

Let $u_i^n \cong u(a_i, t^n)$ and $u_{ij}^{n+1} \cong u(M_{ij}, t^{n+1})$ denote the nodal (or cell average) values in the first and second grid at time $t = t^n$ and $t = t^{n+1}$, respectively (n even).

For the barycentric cell C_i, let $\vec{\nu}_{ij}^{\,1}$ and $\vec{\nu}_{ij}^{\,2}$ denote the unit outer normal vectors to $G_{ij}M_{ij}$ and $M_{ij}G_{i,j+1}$ respectively, pointing out of cell C_i (Fig. 4), and for the quadrilateral cell L_{ij}, let $\vec{n}_{ij}^{\,1}, \ldots, \vec{n}_{ij}^{\,4}$ be the normal vectors to the cell edges $a_i G_{ij}$, $G_{ij}a_j$, $a_j G_{i,j+1}$ and $G_{i,j+1}a_i$, respectively, pointing out of cell L_{ij} (Fig. 5).

We must also define the elementary flux vectors

$$\vec{\eta}_{ij} = \int_{\Gamma_{ij} = G_{ij}M_{ij}G_{i,j+1}} \vec{\nu}\, d\sigma = |\overrightarrow{G_{ij}M_{ij}}|\vec{\nu}_{ij}^{\,1} + |\overrightarrow{M_{ij}G_{i,j+1}}|\vec{\nu}_{ij}^{\,2} \quad (3.3a)$$

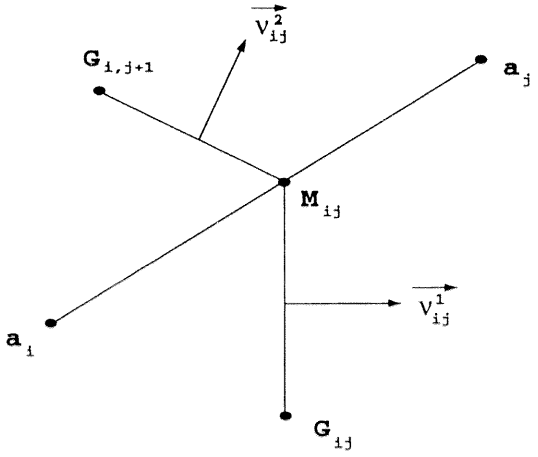

FIGURE 4 Barycentric cell boundary element $\Gamma_{ij} = G_{ij}M_{ij} \cup M_{ij}G_{ij+1}$.

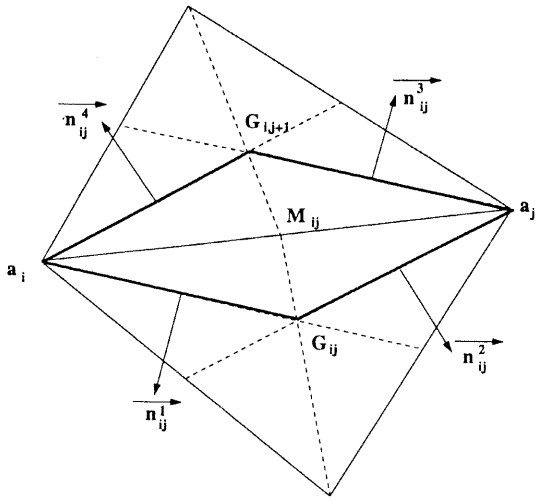

FIGURE 5 Quadrilateral cells L_{ij}.

and

$$\begin{cases} \vec{\theta}_{ij} = |\overrightarrow{a_i G_{ij}}|\vec{n}_{ij}^{\,1} + |\overrightarrow{a_i G_{i,j+1}}|\vec{n}_{ij}^{\,4} \\ \vec{\theta}_{ji} = |\overrightarrow{a_j G_{ij}}|\vec{n}_{ij}^{\,2} + |\overrightarrow{a_i G_{i,j+1}}|\vec{n}_{ij}^{\,3}. \end{cases} \quad (3.3b)$$

We write furthermore

$$\vec{\nu}_{ij}^{\,k} = \begin{pmatrix} \nu_{ijx}^k \\ \nu_{ijy}^k \end{pmatrix} \text{ for } k = 1, 2,$$

$$\vec{n}_{ij}^{\,k} = \begin{pmatrix} n_{ijx}^k \\ n_{ijy}^k \end{pmatrix} \text{ for } k = 1, \ldots, 4$$

$$\text{and } \vec{\eta}_{ij} = \begin{pmatrix} \eta_{ijx} \\ \eta_{ijy} \end{pmatrix}, \ \vec{\theta}_{ij} = \begin{pmatrix} \theta_{ijx} \\ \theta_{ijy} \end{pmatrix}. \quad (3.3c)$$

An advantage of using a finite volume formulation where the degrees of freedom are values of the unknown function at the triangulation vertices lies in the possibility to couple (3.1) with an elliptic equation. This can be very convenient in the case where

$$\begin{cases} f(u) = w_1 h(u) \\ g(u) = w_2 h(u) \end{cases}$$

i.e. when (3.1) can be written as $u_t + \mathrm{div}(\vec{W} h(u)) = 0$ with $\vec{W} = (w_1, w_2)^T$ and $\vec{W}$ stems from an elliptic problem. This situation arises in the study of polyphase flows in porous media, where fluid mechanical and thermodynamical considerations are combined, leading to coupled hyperbolic and elliptic equations [8].

The first step of the two-dimensional finite volume extension of the Lax-Friedrichs scheme is defined by integrating (3.1) on the 3-dimensional cell $L_{ij} \times [t^n, t^{n+1}]$, assuming that the (barycentric) cell values u_i^n at the vertices a_i of the original triangulation are known:

$$\int_{t^n}^{t^{n+1}} \int_{L_{ij}} (u_t + f(u)_x + g(u)_y) dx dy dt = 0. \quad (3.4a)$$

Applying the divergence theorem and observing that $L_{ij} = (L_{ij} \cap C_i) \cup (L_{ij} \cap C_j)$ we get

$$\int_{L_{ij}} u(x, y, t^{n+1}) dA - \int_{L_{ij} \cap C_i} u(x, y, t^n) dA$$

$$- \int_{L_{ij} \cap C_j} u(x, y, t^n) dA$$

$$+ \int_{t^n}^{t^{n+1}} \int_{\partial L_{ij}} (f(u) n_x + g(u) n_y) d\sigma dt = 0. \quad (3.4b)$$

Since $u(x, t)$ is approximated by u_i^n in C_i, u_j^n in C_j, we can choose the approximation u_i^n on $\partial L_{ij} \cap C_i$ and u_j^n on $\partial L_{ij} \cap C_j$, whence the first step of our finite volume Lax-Friedrichs scheme:

$$A(L_{ij}) u_{ij}^{n+1} - A(L_{ij} \cap C_i) \cdot u_i^n$$

$$- A(L_{ij} \cap C_j) \cdot u_j^n$$

$$+ \Delta t (f(u_i^n) \theta_{ijx} + g(u_i^n) \theta_{ijy})$$

$$+ \Delta t (f(u_j^n) \theta_{jix} + g(u_j^n) \theta_{jiy}) = 0 \quad (3.5)$$

We note that this approximation corresponds to choosing the approximate time derivative

$$u_t \cong \left(u_{ij}^{n+1} - \frac{A(L_{ij} \cap C_i) \cdot u_i^n + A(L_{ij} \cap C_j) \cdot u_j^n}{A(L_{ij})} \right) \Big/ \Delta t. \quad (3.6)$$

For the second step we proceed similarly with the help of the barycentric cells C_i:

$$A(C_i) u_i^{n+2} - \sum_{j \text{ neighbour of } i} A(L_{ij} \cap C_i) u_{ij}^{n+1}$$

$$+ \Delta t \sum_{j \text{ neighbour of } i} (f(u_{ij}^{n+1}) \eta_{ijx} + g(u_{ij}^{n+1}) \eta_{ijy}) = 0 \quad (3.7)$$

where the value of $u(x, y, t^{n+1})$ on the boundary $\partial C_i = \cup_{j \text{ neighbour of } i} \Gamma_{ij}$ is approximated locally, on $\partial C_i \cap L_{ij} = \Gamma_{ij}$, by u_{ij}^{n+1} (i.e. the approximate value of u^{n+1} on the quadrilateral cell L_{ij}. We thus alternately define an approximate solution u_{ij}^{n+1} which is piecewise constant on the quadrilateral cells L_{ij}, at odd time steps ($n = 0, 2, \ldots$), and a solution u_i^{n+2} constant on the barycentric cells C_i, at even time steps.

4. A TWO-DIMENSIONAL FINITE VOLUME EXTENSION OF THE NESSYAHU-TADMOR SCHEME

At the beginning of the $(n+1)^{st}$ time step (n even), we have obtained approximate barycentric cell values u_i^n (a_i: a vertex of $\mathcal{T}_h$). We must now, in order to follow the van Leer MUSCL approach used by Nessyahu and Tadmor, construct a piecewise linear profile on the barycentric cells C_i; this can be achieved as follows.

We first construct a piecewise linear approximant on each triangle T of the original triangulation, continuous on the whole computational domain Ω_h, with the help of the barycentric cell/nodal values u_i^n: If $T \in \mathcal{T}_h$ is a triangle with vertices a_{i_j}, $(j = 1, 2, 3)$, we construct $p_T \in P^1$ such

that

$$p_T(a_{ij}) = u_{i_j}^n (j = 1, 2, 3)$$

$p_T(x, y)$ is easily obtained from the barycentric coordinates of (x, y) with respect to the vertices of T:

$$p_T(\vec{x}) = \sum_{j=1}^{3} \lambda_j(\vec{x}) u_j^n$$

where the vertices of T have been relabelled $1, 2, 3$ or a_1, a_2, a_3, and $\vec{x} = (x, y) \in T$.

The gradient of the (barycentric) cellwise *piecewise linear interpolant* $L(x, y, t^n)$ to be defined will now be chosen (as e.g. in [9] p.28), for cell C_i, as the arithmetic average of the gradients of the polynomials p_T for all triangles T such that $a_i \in T$: on C_i we take

$$L = L_i(x, y, t^n) = u_i^n + (x - x_i) P_i^n + (y - y_i) Q_i^n \quad (x, y) \in C_i \tag{4.1a}$$

where

$$\begin{pmatrix} P_i^n \\ Q_i^n \end{pmatrix} = \underset{a_i \in T}{\text{Average}} \{\text{grad } p_T\}. \tag{4.1b}$$

Contrary to what prevailed in the one-dimensional case, where the average value $\bar{u}_j^n$ of the piecewise linear interpolant $L_j(x, t^n)$ was also its value at the node x_j, we can no longer identify the average value of the piecewise linear interpolant (4.1), on cell C_i, with its nodal value u_i^n at the "center" a_i of C_i, since a_i need not be the centroid of C_i, and $(1/A(C_i)) \int_{C_i} L_i(x, y, t^n) dA \neq u_i^n$ in general.

The new cell values at t^{n+1} and t^{n+2} will nevertheless again be *defined* by formulas similar to (2.13) and (3.4b), (3.5) (first step), and (3.7) (second step), obtained by integrating (3.1) on $L_{ij} \times [t^n, t^{n+1}]$ for the first step, and on $C_i \times [t^n, t^{n+1}]$ for the second step:

$A(L_{ij}) u_{ij}^{n+1} \equiv$ numerical approximation of

$$\int_{L_{ij}} u(x, y, t^{n+1}) dA \tag{4.2a}$$

$A(C_i) u_i^{n+2} \equiv$ numerical approximation of

$$\int_{C_i} u(x, y, t^{n+2}) dA. \tag{4.2b}$$

For the first step of our scheme we write

$$\int_{t^n}^{t^{n+1}} \int_{L_{ij}} (u_t + f(u)_x + g(u)_y) dA dt = 0 \tag{4.3a}$$

which leads to

$$\int_{L_{ij}} u(x, y, t^{n+1}) dA = \int_{L_{ij} \cap C_i} L(x, y, t^n) dA + \int_{L_{ij} \cap C_j} L(x, y, t^n) dA - \int_{t^n}^{t^{n+1}} \int_{\partial L_{ij}} (f(u) n_x + g(u) n_y) d\sigma dt. \tag{4.3b}$$

The numerical approximation of the right-hand side, and (4.2a), will thus lead to u_{ij}^{n+1}, which will be our cell value for the quadrilateral cell L_{ij}.

4.1. Approximation of $\int_{L_{ij} \cap C_i} L(x, y, t^n) dA$

$L(x, y, t^n)$ is the piecewise linear function defined, on cell C_i, by (4.1). Let $A_i A_{ij} B_{ij} A_{i,j+1}$ be the points of the plane defined by the linear function L_i on C_i which correspond to the four vertices of $L_{ij} \cap C_i = [a_i G_{ij} M_{ij} G_{i,j+1}]$ where $[\cdots]$ denotes the quadrilateral generated by the corresponding vertices (Fig. 6).

The integral of L on $L_{ij} \cap C_i$ is equal to the total volume of the two prisms with triangular base $a_i G_{ij} M_{ij} A_i A_{ij} B_{ij}$ and $a_i M_{ij} G_{i,j+1} A_i B_{ij} A_{i,j+1}$, constructed on the triangular bases $L_{ij}^r \cap C_i$ and $L_{ij}^\ell \cap C_i$ where $L_{ij}^r =$ triangle $(a_i G_{ij} a_j)$ and $L_{ij}^\ell =$ triangle $(a_i a_j G_{i,j+1})$; r, ℓ stand for right, left (for an observer at a_i).

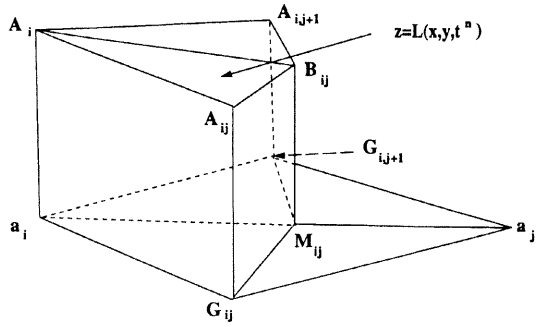

FIGURE 6 Prismatic regions for the computation of $\int_{L_{ij}\cap C_i} L(x, y, t^n) dA$.

The volume of the first prism, for instance, is given by

$$\begin{aligned}
&\mathrm{Vol}\{a_i G_{ij} M_{ij} A_i A_{ij} B_{ij}\} \\
&= \frac{1}{3}\mathrm{Area}(a_i G_{ij} M_{ij}) \\
&\quad \cdot [a_i A_i + G_{ij} A_{ij} + M_{ij} B_{ij}] \\
&= \frac{1}{3}\mathrm{Area}(L_{ij}^r \cap C_i)\{u_i^n + u_i^n + (x_{G_{ij}} - x_i) P_i^n \\
&\quad + (y_{G_{ij}} - y_i) Q_i^n + u_i^n + (x_{M_{ij}} - x_i) P_i^n \\
&\quad + (y_{M_{ij}} - y_i) Q_i^n\} \\
&= \mathrm{Area}(L_{ij}^r \cap C_i)\left\{u_i^n + \frac{1}{3}(x_{G_{ij}} + x_{M_{ij}} - 2x_i) P_i^n \right. \\
&\quad \left. + \frac{1}{3}(y_{G_{ij}} + y_{M_{ij}} - 2y_i) Q_i^n\right\} \qquad (4.4a)
\end{aligned}$$

where

$$\begin{aligned}
\mathrm{Area}(L_{ij}^r \cap C_i) &\equiv \text{Area triangle } (a_i G_{ij} M_{ij}) \\
&= \frac{1}{2}\{(x_{G_{ij}} - x_i)(y_{M_{ij}} - y_i) - (x_{M_{ij}} - x_i)(y_{G_{ij}} - y_i)\}. \qquad (4.4b)
\end{aligned}$$

Similarly, the volume of the second prism is

$$\begin{aligned}
&\mathrm{Vol}\{a_i M_{ij} G_{i,j+1} A_i B_{ij} A_{i,j+1}\} \\
&= \mathrm{Area}(L_{ij}^{\ell} \cap C_i) \cdot \\
&\left\{u_i^n + \frac{1}{3}(x_{M_{ij}} + x_{G_{i,j+1}} - 2x_i) P_i^n \right. \\
&\left. + \frac{1}{3}(y_{M_{ij}} + y_{G_{i,j+1}} - 2y_i)\right\} \qquad (4.4c)
\end{aligned}$$

Summing (4.4a) and (4.4c), we get

$$\begin{aligned}
&\int_{L_{ij}\cap C_i} L(x, y, t^n) dA = \mathrm{Area}(L_{ij} \cap C_i) \cdot \\
&\left\{u_i^n + \frac{1}{3}(x_{M_{ij}} - x_i) P_i^n + \frac{1}{3}(y_{M_{ij}} - y_i) Q_i^n\right\} \\
&+ \frac{1}{3}\mathrm{Area}(L_{ij}^r \cap C_i)\{(x_{G_{ij}} - x_i) P_i^n \\
&+ (y_{G_{ij}} - y_i) Q_i^n\} \\
&+ \frac{1}{3}\mathrm{Area}(L_{ij}^{\ell} \cap C_i)\{(x_{G_{i,j+1}} - x_i) P_i^n \\
&+ (y_{G_{i,j+1}} - y_i) Q_i^n\} \qquad (4.5a)
\end{aligned}$$

with

$$\begin{aligned}
\mathrm{Area}(L_{ij}^{\ell} \cap C_i) = \frac{1}{2}\{&(x_{M_{ij}} - x_i)(y_{G_{i,j+1}} - y_i) \\
&- (x_{G_{i,j+1}} - x_i)(y_{M_{ij}} - y_i)\}. \qquad (4.4d)
\end{aligned}$$

4.2. Approximation of $\int_{L_{ij}\cap C_j} L(x, y, t^n) dA$

Proceeding in the same way we find

$$\int_{L_{ij}\cap C_j} L(x, y, t^n)\, dA = \mathrm{Area}(L_{ij} \cap C_j) \cdot$$

$$\left\{u_j^n+\frac{1}{3}(x_{M_{ij}}-x_j)P_j^n+\frac{1}{3}(y_{M_{ij}}-y_j)Q_j^n\right\}$$

$$+\frac{1}{3}\text{Area}(L_{ij}^r\cap C_j)\{(x_{G_{ij}}-x_j)P_j^n$$

$$+(y_{G_{ij}}-y_j)Q_j^n\}$$

$$+\frac{1}{3}\text{Area}(L_{ij}^{\prime}\cap C_j)\{(x_{G_{i,j+1}}-x_j)P_j^n$$

$$+(y_{G_{i,j+1}}-y_j)Q_j^n\} \tag{4.5b}$$

where

$$\text{Area}(L_{ij}^r\cap C_j)=\frac{1}{2}\{(x_{M_{ij}}-x_j)(y_{G_{ij}}-y_j)$$

$$-(x_{G_{ij}}-x_j)(y_{M_{ij}}-y_j)\}.$$

4.3. Approximation of $\int_{t^n}^{t^{n+1}}\int_{\partial L_{ij}}\{f(u)n_x+g(u)n_y\}d\sigma\,dt$

This is achieved with the midpoint rule for integration with respect to time:

$$\int_{t^n}^{t^{n+1}}\int_{\partial L_{ij}}(f(u)n_x+g(u)n_y)d\sigma\,dt$$

$$\cong\Delta t\int_{\partial L_{ij}}\{f(u(x,y,t^{n+1/2}))n_x$$

$$+g(u(x,y,t^{n+1/2}))n_y\}d\sigma \tag{4.5c}$$

where a first order Taylor expansion is used for $u(x,y,t^{n+1/2})$; using (3.1) we write

$$u(x,y,t^{n+1/2})\cong(x,y,t^n)$$

$$-\frac{\Delta t}{2}\{f'(u(x,y,t^n))u_x(x,y,t^n)$$

$$+g'(u(x,y,t^n))u_y(x,y,t^n)\} \tag{4.6}$$

On $L_{ij}\cap C_i$, we have chosen $u_x\equiv P_i^n$ and $u_y\equiv Q_i^n$, but we must find an approximate value of $u(x,y,t^n)$ on the line segments a_iG_{ij} and $a_iG_{i,j+1}$ (and similarly on a_iG_{ij} and $a_jG_{i,j+1}$). One possible choice consists in choosing the value of $L(x,y,t^n)$, our linear interpolant, at the midpoints of these segments, we then take, for any (x,y) on a_iG_{ij}:

$$u(x,y,t^n)\cong u_i^n+\frac{1}{2}(x_{G_{ij}}-x_i)P_i^n$$

$$+\frac{1}{2}(y_{G_{ij}}-y_i)Q_i^n\equiv u_{a_i,G_{ij}}^n \tag{4.7}$$

thus defining our value $u_{a_i,G_{ij}}^n$ for the side a_iG_{ij} of L_{ij}.

In view of (4.6), we can now define an approximate average value of $u(x,y,t^{n+1/2})$ along the side a_iG_{ij} to be used in (4.5c):

$$u_{a_iG_{ij}}^{n+1/2}=u_{a_i,G_{ij}}^n-\frac{\Delta t}{2}\{f'(u_{a_i,G_{ij}}^n)P_i^n+g'(u_{a_i,G_{ij}}^n)Q_i^n\}.$$

Introducing these values in (4.5c), we finally get

$$\frac{1}{\Delta t}\int_{t^n}^{t^{n+1}}\int_{\partial L_{ij}}\{f(u)n_x+g(u)n_y\}d\sigma\,dt$$

$$\cong f(u_{a_i,G_{ij}}^{n+1/2})n_{ijx}^1\cdot|a_iG_{ij}|+f(u_{a_i,G_{i,j+1}}^{n+1/2})n_{ijx}^4\cdot|a_iG_{i,j+1}|$$

$$+f(u_{a_j,G_{ij}}^{n+1/2})n_{ijx}^2\cdot|a_jG_{ij}|+f(u_{a_j,G_{i,j+1}}^{n+1/2})n_{ijx}^3\cdot|a_jG_{i,j+1}|$$

$$+g(u_{a_i,G_{ij}}^{n+1/2})n_{ijy}^1\cdot|a_iG_{ij}|+g(u_{a_i,G_{i,j+1}}^{n+1/2})n_{ijy}^4\cdot|a_iG_{i,j+1}|$$

$$+g(u_{a_j,G_{ij}}^{n+1/2})n_{ijy}^2\cdot|a_jG_{ij}|+g(u_{a_j,G_{i,j+1}}^{n+1/2})n_{ijy}^3\cdot|a_jG_{i,j+1}|. \tag{4.5e}$$

4.4. First Step of the Finite Volume Extension of the Nessyahu-Tadmor Scheme

Collecting our approximations (4.5a, b, e) of the three terms appearing in the R.H.S. of (4.3b) and taking (4.2a) into account, we obtain the following

approximation u_{ij}^{n+1} for the first (odd) time step of our scheme:

$$\text{Area}(L_{ij})u_{ij}^{n+1} = \text{R.H.S.(4.5a)} + \text{R.H.S.(4.5b)} - \Delta t \cdot \{\text{R.H.S.(4.5e)}\} \quad (4.8)$$

where u_{ij}^{n+1} can be considered as a cell value for cell L_{ij} at time t^{n+1}, or as a nodal value at the midpoint M_{ij}, at time t^{n+1}.

In preparation for the second (even) time step, we now construct a piecewise linear approximation of u on the quadrilaterals L_{ij}:

$$u(x, y, t^{n+1}) \cong L^{(o)}(x, y, t^{n+1}) \equiv u_{ij}^{n+1} + (x - x_{M_{ij}})P_{ij}^{n+1} + (y - x_{M_{ij}})Q_{ij}^{n+1} \quad (4.9)$$

where the slopes P_{ij}^{n+1}, Q_{ij}^{n+1} can be computed as follows.

First we construct a piecewise linear approximate function defined on the triangles $T \in \mathcal{T}_h$ of the original triangulation. On triangle $T = a_i a_j a_k$, we can use for that purpose the newly obtained values u_{ij}^{n+1} at the midpoints of the sides of T. We then compute the average of the slopes of the linear interpolants in the two triangles $T, T' \in \mathcal{T}_h$ sharing $a_i a_j$ as a common side (Fig. 5), and use these averages in (4.9).

4.5. Second Step of the Finite Volume Extension of the Nessyahu-Tadmor Scheme

The second step is obtained by integrating (3.1) on the cylindric region $C_i \times [t^{n+1}, t^{n+2}]$, using the same finite volume approach as for the first step, to define a cell average value u_i^{n+2} on cell C_i:

$$\text{Area}(C_i)u_i^{n+2} - \sum_{j \text{ neighbour of } i} \int_{L_{ij} \cap C_i} u(x, y, t^{n+1})\,dx\,dy = -\Delta t \sum_{j \text{ neighbour of } i} \int_{\Gamma_{ij}} \{f(u(x, y, t^{n+3/2}))v_x + g(u(x, y, t^{n+3/2}))v_y\}\,d\sigma \quad (4.10)$$

where $u(x, y, t^{n+1})$ is approximated, on $L_{ij} \cap C_i$, by the piecewise linear interpolant (4.9). Its integral on $L_{ij} \cap C_i$ is computed as described in section 4.1.

To obtain an approximate value of $u(x, y, t^{n+3/2})$ we use a Taylor expansion with respect to time combined with (3.1), and we subdivide the cell-boundary element Γ_{ij} into $G_{ij}M_{ij} \cup M_{ij}G_{i,j+1}$. On $G_{ij}M_{ij}$ (resp. $M_{ij}G_{i,j+1}$), $u(x, y, t)$ is then approximated by its value of the midpoint of the line segment $G_{ij}M_{ij}$ (resp. $M_{ij}G_{i,j+1}$).

4.6. Approximation of the Slopes

In order to compute the gradient (P_i^n, Q_i^n) of the piecewise linear interpolant $L(x, y, t^n)$ for the cell C_i, we must first compute the gradient of the first degree polynomials P_T for all triangles $T \in \mathcal{T}_h$ such that $a_i \in T$. Although we could then in principle directly take the average of the gradients of the polynomials P_T, obtained as described at the beginning of section 4, we shall consider here a least-squares technique (cf. [7]). For simplicity, we shall describe it for the case of triangular (finite volume) cells.

Let T be a triangle with centroid G, and let T_j, $j = 1, 2, 3$ be the neighbouring triangles, with centroids $G_j (j = 1, \ldots, 3)$ (Fig. 7); assume the values of the numerical approximation of the solution u at

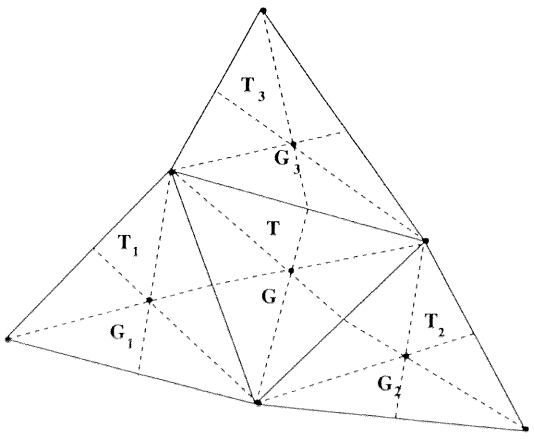

FIGURE 7 Computation of the least-squares gradient for a triangular cell T.

the four points $\{G, G_j\}_{j=1}^3$ are known at time t^n, equal to $u_T^n, u_{T_j}^n (j = 1, \ldots, 3)$ (these values can be considered as cell values playing for the triangular cells T, T_j the same role as u_i^n, u_{ij}^n for the cells C_i, L_{ij}).

The least-squares gradient $\widetilde{(\text{grad } u)}_T^n = (\tilde{a}_T^n, \tilde{b}_T^n)$ for triangle T will then be chosen such as to minimize the functional

$$I = \sum_{j=1}^{3} \{u_T^n + \overrightarrow{GG_j} \cdot (\text{grad } u)_T^n - u_{T_j}^n\}^2 \qquad (4.11)$$

where

$$(\text{grad } u)_T^n = (a_T^n, b_T^n)$$

The minimum is obtained when

$$\frac{\partial I}{\partial a_T^n} = \frac{\partial I}{\partial b_T^n} = 0 \qquad (4.12)$$

and is shown in [7] to lead to the following least-squares gradient:

$$\tilde{a}_T^n = \frac{1}{D} \sum_{j=1}^{3} (y_{G_j} - y_G)^2 \sum_{j=1}^{3} (u_{T_j}^n - u_T^n)(x_{G_j} - x_G)$$

$$- \frac{1}{D} \sum_{j=1}^{3} (x_{G_j} - x_G)(y_{G_j} - y_G) \sum_{j=1}^{3} (u_{T_j}^n - u_T^n)(y_{G_j} - y_G) \qquad (4.13a)$$

$$\tilde{b}_T^n = \frac{1}{D} \sum_{j=1}^{3} (x_{G_j} - x_G)^2 \sum_{j=1}^{3} (u_{T_j}^n - u_T^n)(y_{G_j} - y_G)$$

$$- \frac{1}{D} \sum_{j=1}^{3} (x_{G_j} - x_G)(y_{G_j} - y_G) \sum_{j=1}^{3} (u_{T_j}^n - u_T^n)(x_{G_j} - x_G) \qquad (4.13b)$$

where the denominator

$$D = \sum_{j=1}^{3} (x_{G_j} - x_G)^2 \sum_{j=1}^{3} (y_{G_j} - y_G)^2$$

$$- \left[\sum_{j=1}^{3} (x_{G_j} - x_G)(y_{G_j} - y_G) \right]^2 \qquad (4.13c)$$

is strictly positive for any non-degenerated triangle.

For the barycentric cells C_i or the quadrilateral cells L_{ij}, the procedure is quite similar to the one described above for triangular cells. Alternately, for a barycentric cell C_i with center a_i, we could first compute the least squares gradient grad $u|_{T_j} = (\tilde{a}_{T_j}^n, \tilde{b}_{T_j}^n)$ of each neighbouring triangle T_j (such that $a_i \in T_j$), and then take the cell gradient grad $u|_{C_i} = \text{average } \{\text{grad } u|_{T_j}\}$, with a similar procedure for a quadrilateral cell L_{ij}.

Unfortunately, this procedure does not preserve monotonicity of the data in the usual van Leer sense described below, and allows the creation of local extremas between the nodes; this phenomenon may lead to (or amplify already existing) spurious oscillations, with the associated loss of stability and convergence difficulties in the case of steady flows. We have therefore introduced some slope limitation in the computation of the gradients.

4.6.1. Slope Limitation

To ensure the stability of the scheme and prevent the generation of oscillations in regions of strong gradients, we must perform a slope correction. Following van Leer's approach ([11], [12]), in which the value at some interface point $x_{i+1/2}$ (in the one dimensional case) must fall within the range of values spanned by the adjacent grid averages, u_{i-1} and u_{i+1}, we limit the slopes of the linear interpolant L defined by (4.1) (resp. $L^{(o)}$ defined by (4.9)) to ensure that its value at the boundary points $G_{ij}, M_{ij}, G_{i,j+1}$ of ∂C_i (resp. at the vertices $a_i, a_j, G_{ij}, G_{i,j+1}$ of ∂L_{ij}) are bounded by the values at the cell center u_i^n (resp. u_{ij}^{n+1}) and the value u_j^n at the corresponding neighbouring node a_j (resp. $u_{i,j-1}^{n+1}$ and $u_{i,j+1}^{n+1}$ at the adjacent quadrilateral cell "midpoints" $M_{i,j-1}$ and $M_{i,j+1}$).

The limitation procedure is implemented on each cell as follows. Let

$$(\text{grad } u)_i = (P_i, Q_i)^T$$

denote the gradient for cell i, where $P_i \approx u_x, Q_i \approx u_y$ at node i. If u satisfies the van Leer requirement we choose

$$P_i^{\lim} = \underset{j \in \mathcal{N}(i)}{\text{mid mod}} \{P_j\}$$

$$= \begin{cases} \min_{j \in \mathcal{N}(i)} |P_j|. & \text{(common sign of all values } P_j \text{)} \\ & \text{if all the values } P_j (j \in \mathcal{N}(i)) \\ & \text{have the same sign} \\ 0 & \text{otherwise} \end{cases}$$

where $\mathcal{N}(i)$ is the set of nodes j adjacent to node i. If u does not satisfy the van Leer requirement, we set $P_i^{\lim} = 0$. The computation of $Q_i^{\lim}$ is done in the same manner. For quadrilateral cells L_{ij} we proceed in a similar way.

5. NUMERICAL EXPERIMENTS

The extension to two-dimensional systems of conservation laws is achieved following the procedure described in [1], [2], [5]. In [32], the first author had proposed a finite volume extension of the Nessyahu-Tadmor central difference scheme to 2-dimensional rectangular grids. With his student D. Stanescu, and the second author, he then applied this finite volume scheme to **regular rectangular grids** [21]. Some early numerical experiments (Linear advection, Burgers' equation, Diffraction of a planar shock wave around a 90° corner [22], Mach 3 wind tunnel with a forward facing step) confirmed the non-oscillatory character as well as the 2nd-order accuracy of the new scheme [21], while computing times were significantly shorter than corresponding times for Godunov's method.

In this paper, we present sample results from some further numerical experiments with our extension of the Nessyahu-Tadmor scheme to **unstructured triangular** FEM grids [6].

The aim here was not to obtain an optimal accuracy to computing time ratio but simply to show the feasibility of the method. Sharper results, including comparison of results obtained with different limiters, will be described in future work [29].

The overall quality of the results and the relatively low level of both the computational complexity and computing times suggest that two-dimensional problems can be handled very efficiently with our method, which should benefit from its multi-dimensional character, as may be seen from the examples presented here.

Example 1 Linear Advection Problem To test the (predictably) rather unsatisfactory accuracy of our finite volume extension of the Lax-Friedrichs scheme (first order accurate), and compare it to that of our second order accurate finite volume method inspired by the Nessyahu-Tadmor scheme, we solved the linear advection problem

$$u_t + u_x + u_y = 0 \quad -1 \leqslant x,\ y \leqslant 1$$

$$u_o(x, y) = \begin{cases} 0.5 & \text{if } x^2 + y^2 \leqslant 0.5; \\ 0 & \text{otherwise.} \end{cases} \tag{5.1}$$

For this first test case, we felt it might be interesting to show the results obtained with our finite volume extensions of the Lax-Friedrichs and Nessyahu-Tadmor schemes for rectangular grids, with three different choices for the gradients used in the piecewise linear reconstruction at the beginning of each time step, for the second order scheme. We thus tested the following schemes [21].

1) $L \times F$: 2-dimensional staggered finite volume extension of the Lax-Friedrichs scheme (first-order accurate),
2) STG: 2-dimensional Arminjon-Viallon finite volume extension of the Nessyahu-Tadmor scheme with Min-Mod limiter [17],
3) STG-Roe: same as 2, but with Roe's superbee limiter [17],
4) STG-UNO: same as 2, but with UNO- computed slopes (see [21], [13]).

Scheme 1 is first order accurate, while 2, 3 and 4 are second order accurate. The solution at time $t = 0.1$ is computed using 50 double time steps (50

integrations on the staggered grid and 50 on the original grid) on a regular 85×85 rectangular grid, with a CFL-number $v_x = v_y = 0.002$.

The exact solution is

$$u(x, y, t) = u_o(x - t, y - t)$$

and is truly two-dimensional since its wave front is at an angle of 45° with the x and y axes.

Table I shows the L^2-norms of the errors, and thus the increasing accuracy obtained, for this example, with the four schemes.

Figure 8 a), b), c) shows the initial function and the results obtained with the schemes STG and $L \times F$, while Figure 8 d), e) shows the solution $u(x, y = 0, t = 0.1)$ as obtained with STG-UNO and $L \times F$ respectively.

Example 2 A Standard Test Case Euler Flow Around a NACA 0012 Airfoil We present results for the NACA 0012 airfoil at Mach number $M_\infty = 2.0$ and incidence $\alpha = 0°$. The initial mesh

TABLE I L^2-norms of the errors

Scheme	$\|e\|_2$
$L \times F$	$3.055\,E^{-2}$
STG	$1.313\,E^{-2}$
STG-Roe	$8.071\,E^{-3}$
STG-UNO	$6.357\,E^{-3}$

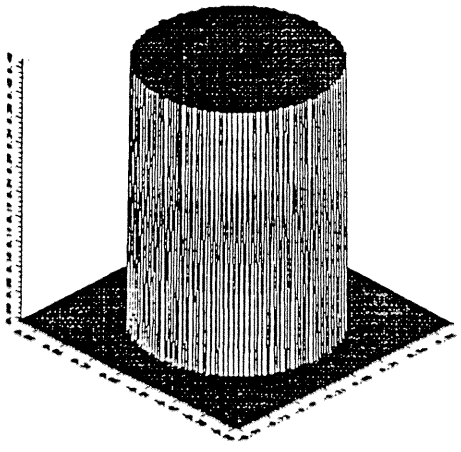

FIGURE 8a Linear advection problem (a) initial distribution.

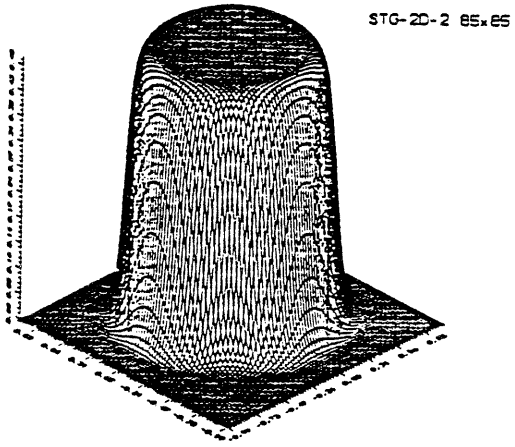

FIGURE 8b Convected surface (STG).

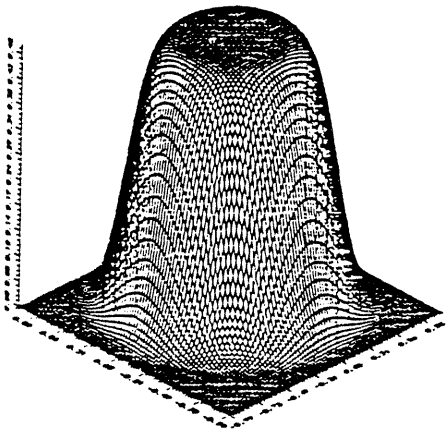

FIGURE 8c Convected surface ($L \times F$).

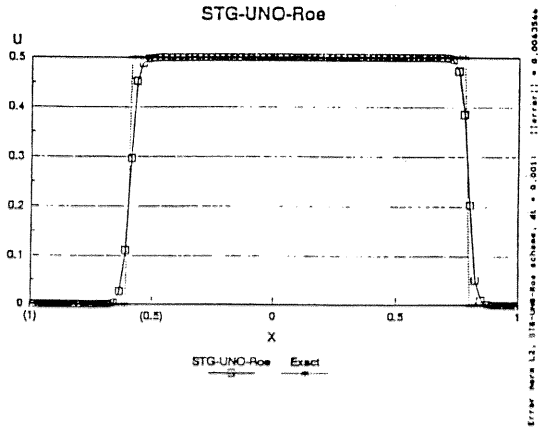

FIGURE 8d Vertical cut of the convected surface (STG-UNO) $y = 0, t = 0.1$.

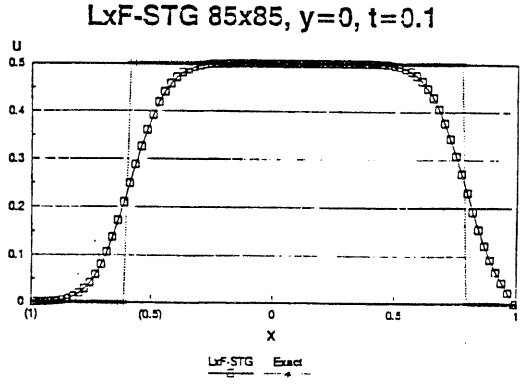

FIGURE 8e Vertical cut of the convected surface $(L \times F)$ $y = 0, t = 0.1$.

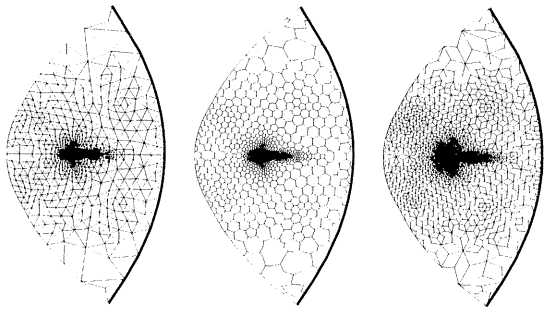

FIGURE 9 Euler flow around a NACA 0012 airfoil. Original grid, barycentric cells C_i and quadrilateral cells L_{ij}.

had 2274 nodes and 4360 elements (Fig. 9 and 10). We observe a reasonably good capture of the shock (Fig. 10) as compared e.g. with [25], where the grid has 4224 nodes. Going to the first improved grid (3557 vertices, Fig. 12) lets our scheme produce a substantially better shock resolution than that displayed in [25]. As we go on, improving the mesh to 4497 vertices (Fig. 13) we observe an even better resolution. The final grid (7269 vertices, Fig. 14) leads to an excellent shock resolution.

The grid adaptation procedure used here has been developed by M. J. Castro Diaz and F. Hecht at INRIA ([30], [31]).

Let us mention, though, that Venkatakrishnan's results are obtained with an implicit scheme using 3 different kinds of limiter; for the best of these, convergence is faster than with our scheme with the basic MinMod limiter; a fact which might be due to the implicit character of the scheme used in [25].

Example 3 Supersonic Flow Past a Double-Ellipse at 20° of Angle of Attack and $M_\infty = 2$ For this problem inspired by ([26]), but with Mach number $M_\infty = 2$ instead of the range of hypersonic Mach numbers considered there, and 20° of angle of attack, the geometry is a double ellipse; it can be defined by

$$\begin{cases} x \leqslant 0 & \begin{cases} z \leqslant 0 & (x/0.06)^2 + (z/0.015)^2 = 1 \\ z \geqslant 0 & (x/0.035)^2 + (z/0.025)^2 = 1 \end{cases} \\ 0 \leqslant x \leqslant 0.016 & \begin{cases} z \geqslant 0 & z = 0.025 \\ z \leqslant 0 & z = -0.015 \end{cases} \end{cases}$$

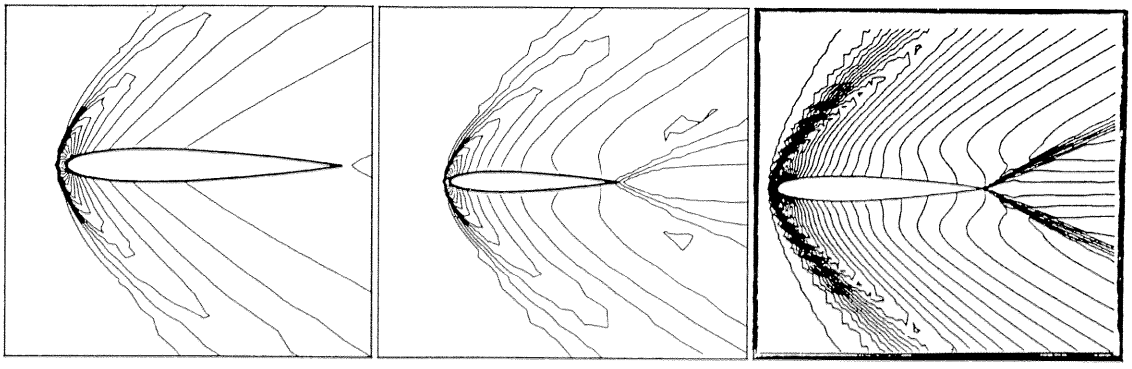

FIGURE 10 NACA 0012 airfoil: Pressure contours (left), Mach contours (middle) (Finite Volume, 2274 vertices); Mach contours with Venkatakrishnan's method (right) (4224 vertices; courtesy of Journal of Computational Physics).

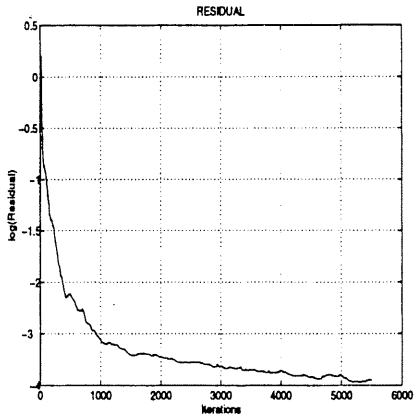

FIGURE 11 Residual for the initial mesh (FV).

tive; we used the same three meshes with both methods. For the initial mesh (1558 vertices), both methods give fairly comparable results; notice that the C_p curves can be nearly superposed, which is an indication that both methods are indeed doing some reasonable calculation. The same is true for the pressure and Mach contours of both methods, with perhaps a very small advantage for our finite volume method (FV) which gives slightly sharper shocks.

For the intermediate mesh (2792 vertices), the advantage offered by the Finite Volume method becomes a little more obvious on Figures 20 and 21, where the breaches of monotonicity are more

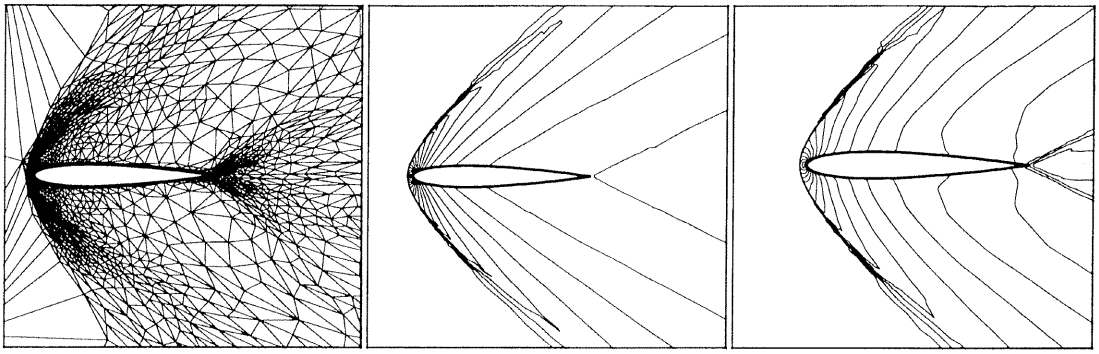

FIGURE 12 NACA0012: First adaptation (3557 vertices) and solution (pressure and Mach contours) (FV).

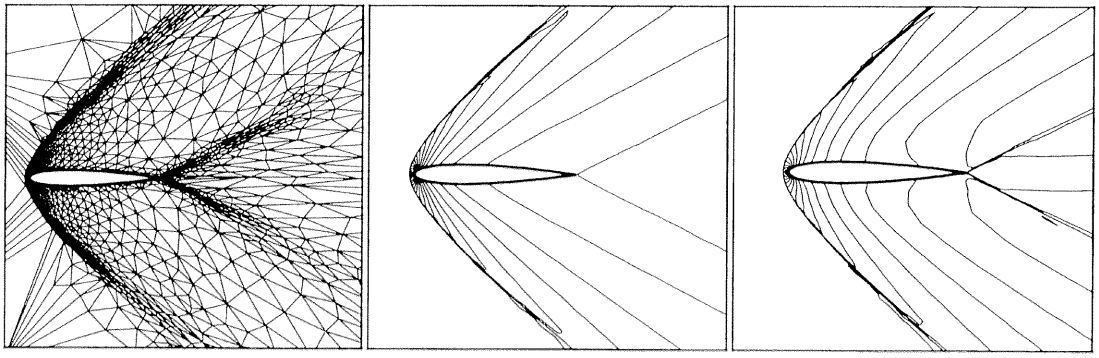

FIGURE 13 NACA0012:2nd adaptation (4497 vertices) and solution (pressure and Mach contours) (FV).

For this steady flow problem we compared our finite volume method with a discontinuous finite element method recently proposed by Jaffré *et al.* ([27], [28]) and which seems to be fairly competi- important with the Discontinuous Finite Element method (DFE) (lower part of the bow shock). Moreover the pressure and Mach contours are more regular with the FV method.

TABLE II The minimal and maximal values of pressure and Mach number (FV)

FV	Pressure		Mach	
Initial mesh	min = 0.1163934	max = 0.9815941	min = $4.1695271e^{-2}$	max = 2.112459
1st mesh	min = 0.1156657	max = 0.9834443	min = $1.0001168e^{-2}$	max = 2.150275
2nd mesh	min = 0.1123134	max = 0.9810082	min = $7.5702323e^{-3}$	max = 2.179578
Final mesh	min = 0.1139615	max = 1.000181	min = $9.072036e^{-3}$	max = 2.320326

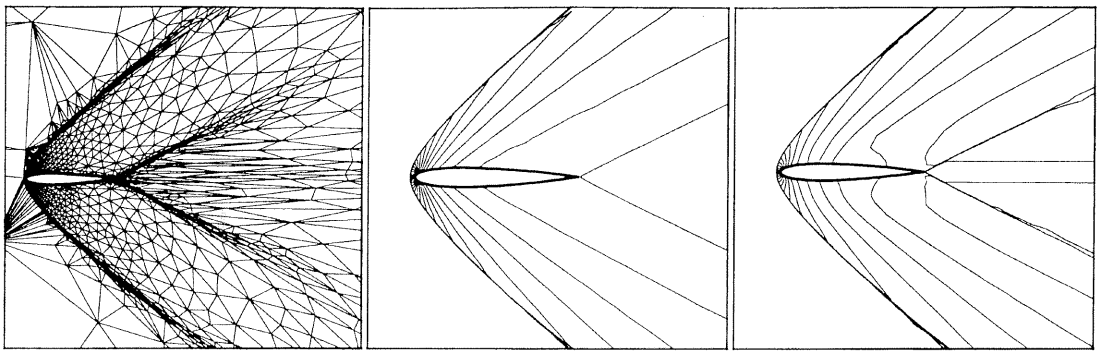

FIGURE 14 NACA0012: Final mesh (7269 vertices) and solution (pressure and Mach contours) (FV).

The final mesh shows a clear advantage for the FV method, which gives a nearly perfect shock resolution with very smooth contours, while the DFE method shows a serious breach of monotonicity in the lower part of the bow shock.

As was the case with the initial mesh, the C_p curves can again be nearly exactly superposed, while the Mach line of the FV method is slightly higher, for the left part of the upper curve, than with the DFE method, a fact which is confirmed by Tables III and IV.

The major difference between the two methods appears to lie in the convergence history and computing times. Figures 17, 20 and 26 show a clear advantage for our finite volume method, for the initial mesh (1558 vertices). Computing times (CPU:3564 for FV and 48288 for DFE) confirm the advantage of the proposed Finite Volume Method. Let us finally mention that all calculations have been performed on a Silicon Graphics Station of the Centre de Recherches Mathématiques (model Challenge, 100 Mhz, 6 processors).

TABLE III Maximal and Minimal values of Pressure and Mach number (FV)

FV	Pressure		Mach	
Initial mesh	min = $6.1671760e^{-2}$	max = 1.009705	min = $1.750865e^{-2}$	max = 2.253697
2nd mesh	min = $6.1395669e^{-2}$	max = 1.006208	min = $5.3774943e^{-3}$	max = 2.266636
Final mesh	min = $6.0346086e^{-2}$	max = 1.009427	min = $5.209895e^{-3}$	max = 2.270716

TABLE IV Maximal and Minimal values of Pressure and Mach number (DFE)

DFE	Pressure		Mach	
Initial mesh	min = $6.2501445e^{-2}$	max = 1.014265	min = $8.2084965e^{-3}$	max = 2.190479
2nd mesh	min = $6.2390134e^{-2}$	max = 1.007068	min = $2.0193825e^{-3}$	max = 2.216612
Final mesh	min = $6.3052103e^{-2}$	max = 1.007425	min = $1.3435918e^{-2}$	max = 2.211899

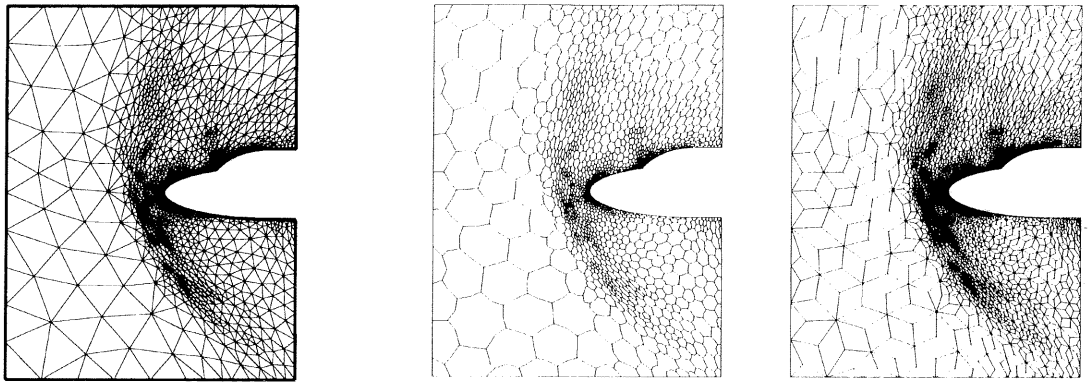

FIGURE 15 Euler flow around a double ellipse. Original grid, barycentric cells C_i and quadrilateral cells L_{ij}.

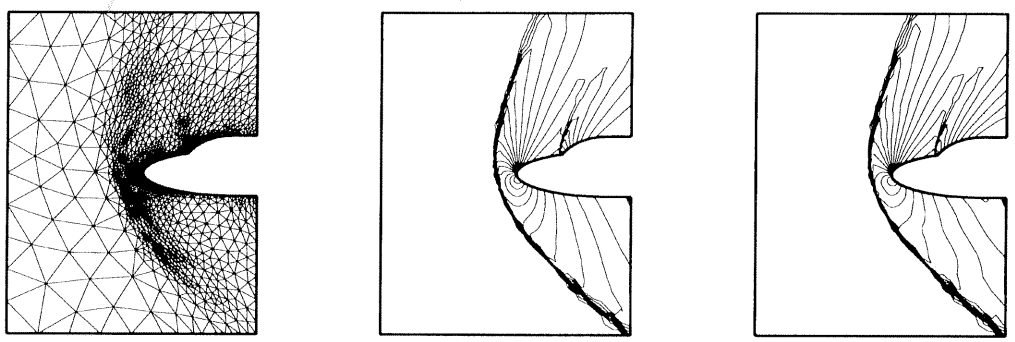

FIGURE 16 Double ellipse: Initial mesh (1558 vertices) and solution (pressure and Mach contours) (FV).

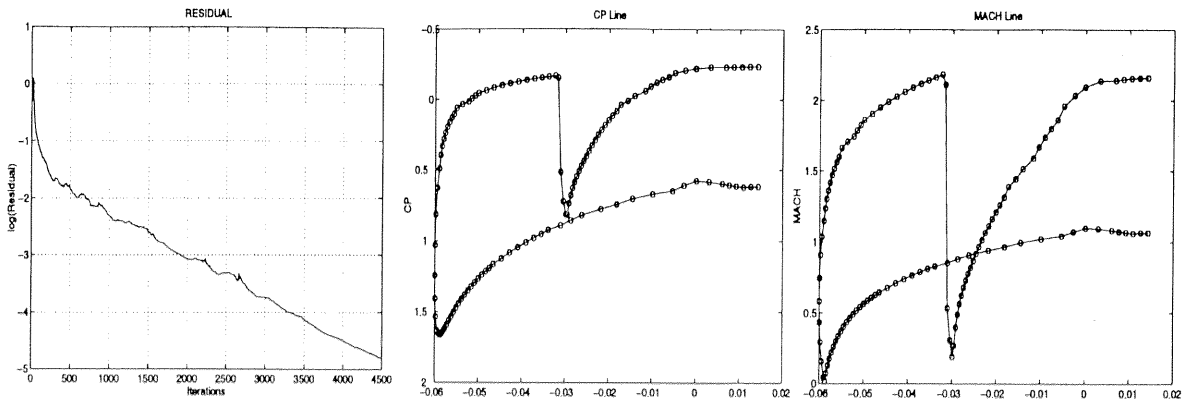

FIGURE 17 Residual and C_p and Mach body cuts (initial mesh 1558 vertices) (FV).

CONCLUDING REMARKS

By first considering two coupled sets of finite volume cells, we have presented a two-dimensional finite volume extension of the Lax-Friedrichs scheme for scalar hyperbolic conservation laws. This scheme has then been used to construct a two-dimensional finite volume generalization of

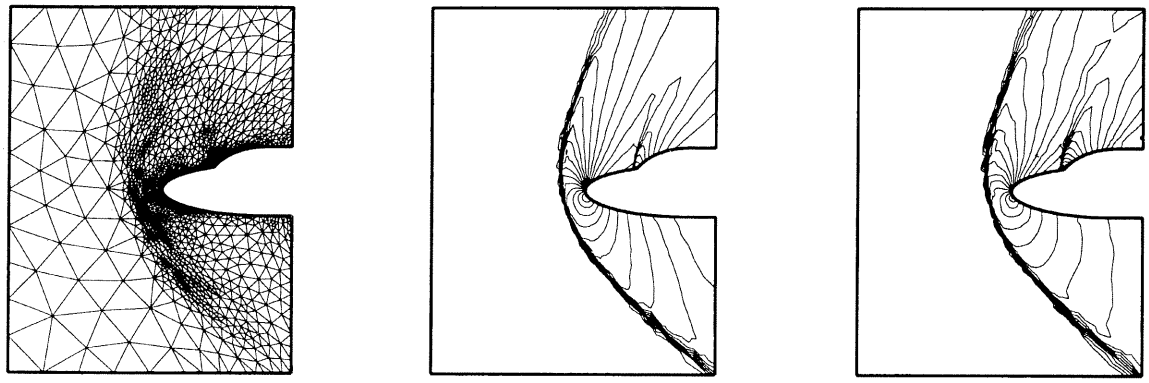

FIGURE 18 Double ellipse: Initial mesh (1558 vertices) and solution (pressure and Mach contours) (DFE).

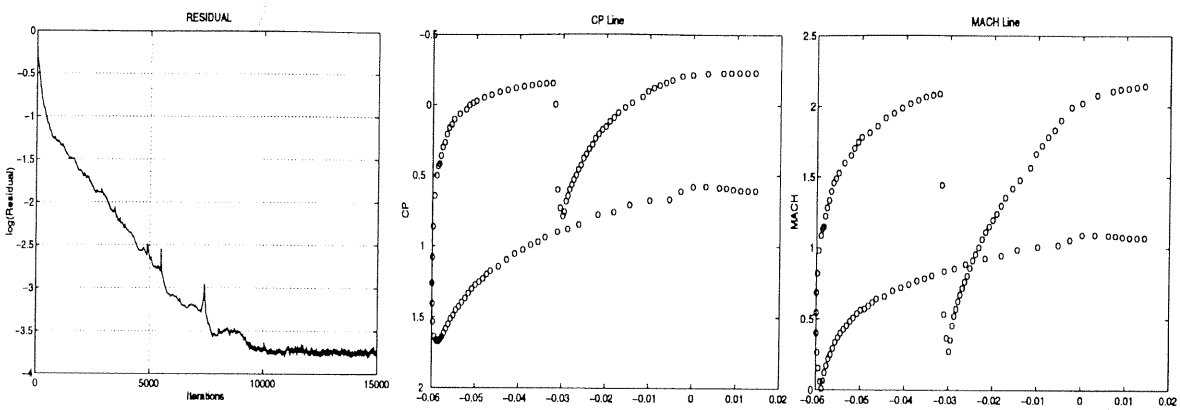

FIGURE 19 Residual and C_p and Mach body cuts (initial mesh 1558 vertices) (DFE).

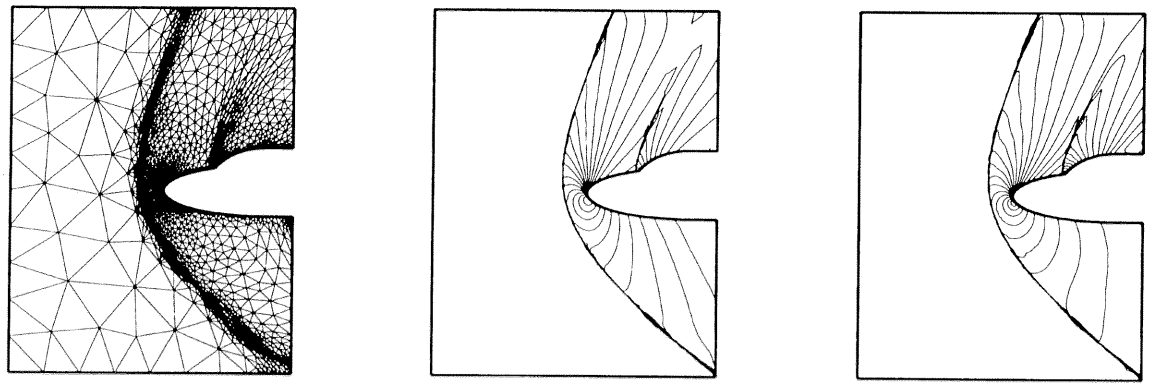

FIGURE 20 Double Ellipse: First adaptation (2792 vertices) and solution (pressure and Mach contours) (FV).

the one-dimensional Nessyahu-Tadmor scheme, thanks to the introduction of van Leer-type two-dimensional piecewise linear interpolants, which leads to second-order accuracy. Oscillations are suppressed with the help of slope or gradient limiters.

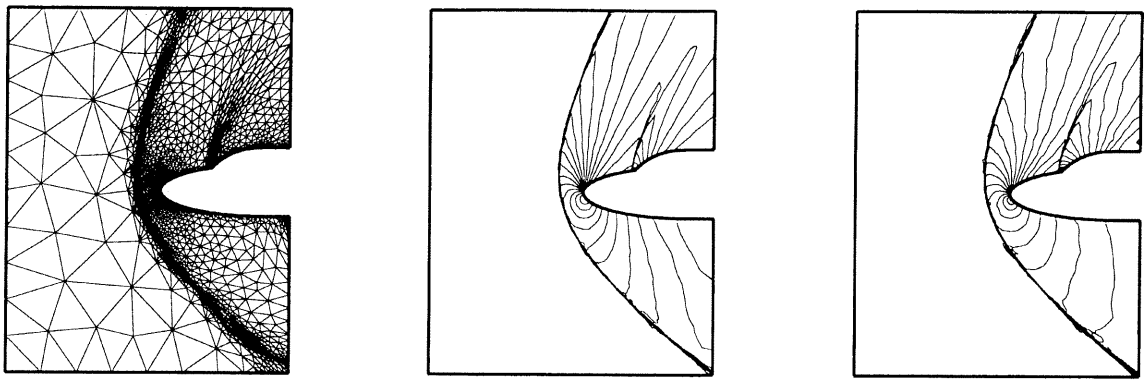

FIGURE 21 Double Ellipse: First adaptation (2792 vertices) and solution (pressure and Mach contours) (DFE).

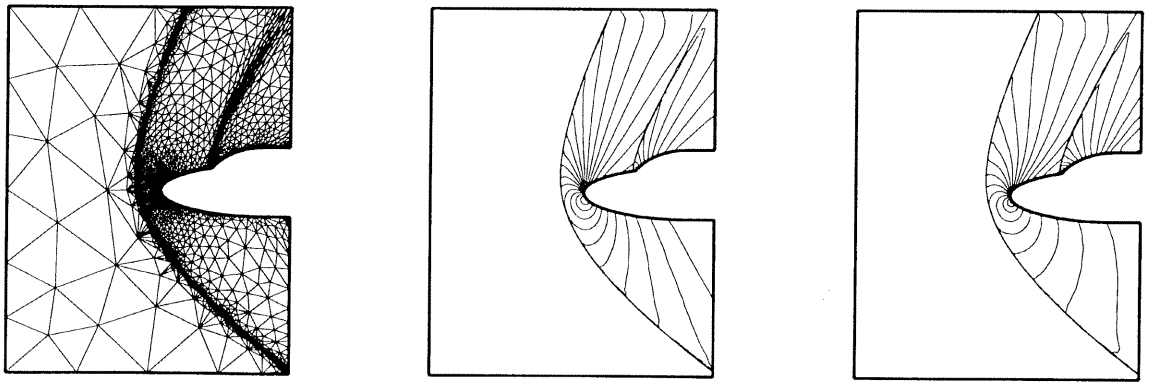

FIGURE 22 Double Ellipse: Final mesh (5055 vertices) and solution (pressure and Mach contours) (FV).

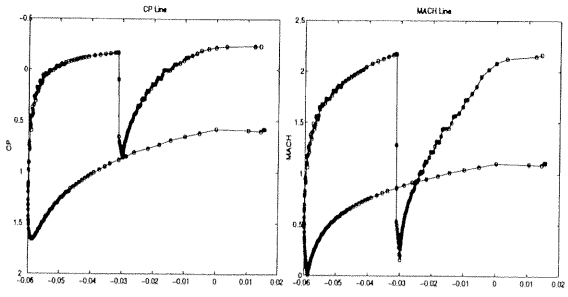

FIGURE 23 C_p and Mach body cuts for the final mesh (5055 vertices) (FV).

The examples presented here give a reasonable evidence that the FV method proposed by the authors is capable of a very high resolution, with a clear advantage, as compared with DFE, at least at the level of the convergence histories, computing times, smoothness of the pressure and Mach contours, and monotonicity enforcement.

In another paper we consider the particular case of the linear equation $u_t + \mathrm{div}(u\vec{V}) = 0$ where $\vec{V} = (V_1(x,y), V_2(x,y))^T$ with $\mathrm{div}\vec{V} = 0$; we obtain an L^∞ bound for the numerical solution, from which we deduct the existence of a subsequence $\{u_{\mathcal{T}_k, \Delta t_k}\}$ which converges weakly to some function u in $L^\infty(\mathbb{R}^2 \times \mathbb{R}^+)$-weak. Using another set of inequalities, we obtain a total variation-type bound, slightly weaker than a classical bound on the total variation of the numerical solution, called *a* bound on the "weighted total variation", from which we are then able to show that the above weak limit function u is indeed a weak solution of $u_t + \mathrm{div}(u\vec{V}) = 0$.

This places the 2-dimensional finite volume generalization of the Nessyahu-Tadmor scheme on a

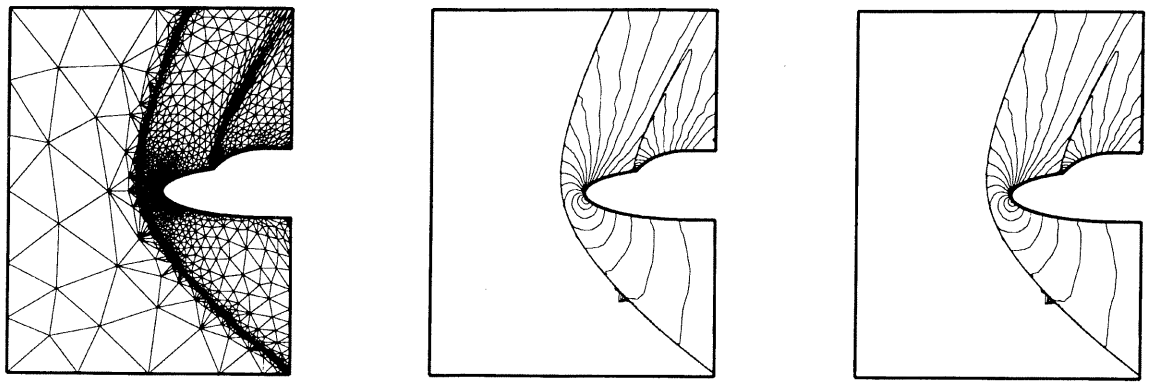

FIGURE 24 Double Ellipse: Final mesh (5055 vertices) and solution (pressure and Mach contours) (DFE).

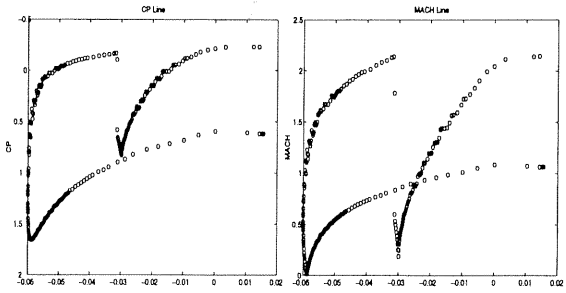

FIGURE 25 C_p and Mach body cuts for the final mesh (5055 vertices) (DFE).

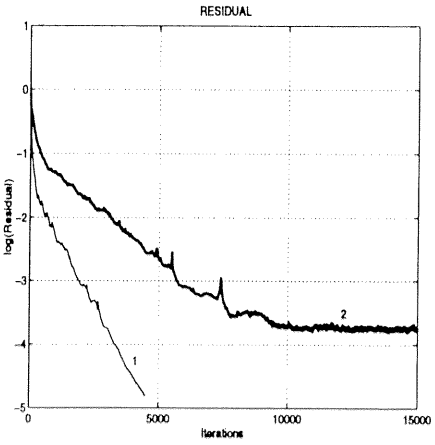

FIGURE 26 Residual for initial mesh (1558 vertices) ((1) = FV – (2) = DFE).

firm theoretical basis, and the authors will now focus their efforts on applications to problems with the Navier-Stokes equations in conservation form for compressible flows and three-dimensional transonic and supersonic flow problems.

Acknowledgements

This research was supported by a grant from the National Science and Engineering Research Council of Canada, and by an FCAR grant from the Government of the Province of Québec.

References

[1] Angrand, F., Dervieux, A., Loth, L. and Vijayasundaram, G. (1983). Simulations of Euler transonic flows by means of explicit finite-element type schemes, INRIA Res. Rep. No. 250, Rocquencourt, 78153 Le Chesnay, France.

[2] Angrand, F. and Dervieux, A. (1984). Some explicit triangular finite element schemes for the Euler equations, *Int. Num. Meth. in Fluids*, **4**, 749–764.

[3] Arminjon, P., Viallon, M. C. and Madrane, A. (1995). From Lax-Friedrichs to a Multidimensional Finite Volume Extension of the Nessyahu-Tadmor Scheme for Compressible Flows, Proc. Int. Conf. on Numerical Meth. for the Euler and Navier-Stokes Equations. Centre de Rech. Math. Univ de Montréal, P. Arminjon and A. Dervieux, editors, september 1995, to appear in the Am. Math. Soc-CRM series.

[4] Arminjon, P., Dervieux, L., Fezoui, L., Steve, H. and Stoufflet, B. (1988). Non-oscillatory schemes for multidimensional Euler calculations with unstructured grids, Proc. 2nd Int. Conf. Hyperbolic Problems, Aachen (Germany), March 1988, R. Jeltsch and J. Ballmann, Editors (Notes on Numer. Fluid Mechanics, **24**, Vieweg, Braunschweig, Germany).

[5] Arminjon, P. and Dervieux, A. (1993). Construction of TVD-like Artificial Viscosities on Two-Dimensional Arbitrary FEM Grids, *J. Comp. Phys.*, **106**, 176–198.

[6] Arminjon, P. and Viallon, M. C. (1995). Généralisation du schéma de Nessyahu-Tadmor pour une équation

hyperbolique à deux dimensions d'espace, Comptes Rendus de l' Acad. des Sciences, Paris, t. 320, série I, 85–88.
[7] Champier, S. (1992). Convergence de schémas numériques type Volumes Finis pour la résolution d'équations hyperboliques. Thèse, Univ. de St-Etienne.
[8] Eymard, R. and Gallouët, T. (1993). Convergence d'un schéma de type éléments finis-volumes finis pour un système d'une équation elliptique et d'une équation hyperbolique, *M^2AN*, **27**(7), 843–861.
[9] Fezoui, F. (1985). Résolution des équations d'Euler par un schéma de van Leer en éléments finis. Rapport INRIA no 358, Rocquencourt, 78153 Le Chesnay, France.
[10] Godunov, S. K. (1959). A Difference Method for the Numerical Computation of Discontinous Solutions of the Equations of Fluid Dynamics, Mat Sbornik., **47**(3), 271–306.
[11] van Leer, B. (1974). Towards the Ultimate Conservative Difference Scheme. II. Monotonicity and conservation combined in a second order scheme, *J. Comp. Phys.*, **14**, 361–370.
[12] van Leer, B. (1977). IV. A new approach to numerical convection, *J. Comp. Phys.*, **23**, 276–299.
[13] Nessyahu, H. and Tadmor, E. (1990). Non-oscillatory Central Differencing for Hyperbolic Conservation Laws, *J. Comp. Physics*, **87**(2), 408–463.
[14] Peyret, R. and Taylor, T. D. (1983). Computational Methods for Fluid Flow, Springer-Verlag, New York, Heidelberg, Berlin.
[15] Roe, P. L. (1981a). The use of the Riemann problem in finite difference schemes, in Proc. 7th *Inter. Conf. Num. Meth. Fluid Dynamics*, Stanford/NASA Ames, W. C. Reynolds and R. Mac Cormack, editors, Lecture Notes in Physics, no 141, Springer-Verlag, New York, 354–359.
[16] Roe, P. L. (1981b). Approximate Riemann solvers, parameter vectors, and difference schemes, *J. Comp. Phys.*, **43**, 357–372.
[17] Sweby, P. K. (1984). High resolution schemes using flux limiters for hyperbolic conservation laws, *SIAM J. Num. Anal.*, **21**, 995–1011.
[18] Viallon, M. C. and Arminjon, P. (1994). Convergence du schéma de Nessyahu-Tadmor sur des maillages non structurés pour une équation hyperbolique linéaire bidimensionnelle, Rapport de recherche No. C.N.R.S. U.R.A. 740, Équipe d'Analyse Numérique, Universités de Lyon et Saint-Étienne, septembre 1994.
[19] Viallon, M. C. and Arminjon, P. (1995). Convergence of a finite volume extension of the Nessyahu-Tadmor scheme on unstructured grids for a two-dimensional linear hyperbolic equation, Rapport de recherche, No. 2239, Centre de Recherches mathématiques, Université de Montréal, January 1995, to appear in *SIAM J. Num. Anal.*
[20] Lax, P. D. (1954). Weak solutions of nonlinear hyperbolic equations and their numerical computation, *Comm. Pure and Applied Math.*, **7**, 159–193.
[21] Arminjon, P., Stanescu, D. and Viallon, M. C. (1995). A two-dimensional finite volume extension of the Lax-Friedrichs and Nessyahu-Tadmor schemes for compressible flows, A Collection of Technical Papers, Proceedings of the 6 th. Int. Symposium on Comp. Fluid Dynamics, Lake Tahoe (Nevada) September 4–8, 1995, M. Hafez, editor, **4**, pp. 7–14.
[22] Quirk, J. J. (1992). A Contribution to the Great Riemann Solver Debate, NASA-ICASE Rep. No. 92-64, Nov. 1992, and *Int. J. Num. Meth. Fluids*, pp. 555–574 (1994).
[23] Peraire, J., Vahdati, M., Morgan, K. and Zienkiewicz, O. C. (1987). Adaptative Remeshing for Compressible Flow Computations, *J. Comp. Phys.*, **72**, 449–466.
[24] Rizzi, A.-Viviand, H. (Eds) (1981). Numerical methods for the computation of inviscid transonic flow with shock waves. Notes on Numerical Fluid Mechanics, **3**, Vieweg, Braunschweig/Wiesbaden, Germany.
[25] Venkatakrishnan, V. (1995). Convergence to Steady State Solutions of the Euler Equations on Unstructured Grids with Limiters, *J. Comp. Phys.*, **118**, 120–130.
[26] INRIA and GAMNI-SMAI (1990). Workshop on hypersonic flows for reentry problems, Problem 6: Flow over a double ellipse, test case 6.1: Non-Reactive Flows. Antibes, France, January 22–25, 1990.
[27] Gowda, G. D. V. and Jaffré, J. (1993). A discontinuous finite element method for non linear scalar conservation laws, INRIA Res. Rep. No. 1848, Rocquencourt, 78153 Le Chesnay, France
[28] Jaffré, J. and Kaddouri, L. (1991). Discontinuous finite elements for the Euler equations. Proc. of the 3rd Int. Conf. on Hyperbolic Problems, June 11–15, 1990, Uppsala, Sweden, B. Engquist and B. Gustafsson, editors, Studentlitteratur, Chartwell-Bratt, **2**, pp. 602–610.
[29] Arminjon, P., Viallon, M. C., Kaddouri, L. and Madrane, A., Discontinuous finite elements and 2-Dimensional Finite Volume Versions of the Lax-Friedrichs and Nessyahu-Tadmor difference schemes for Compressible Flows on Unstructured Grids, to appear in CFD Review, John Wiley, 1997, M. Hafez and K. Oshima, Editors.
[30] Castro Diaz, M. J. and Hecht, F., Anisotropic Surface Mesh Generation, INRIA Res. Rep. No. 2672, October 1995, INRIA, Rocquencourt, 78153 Le Chesnay, France.
[31] Castro Diaz, M. J., Mesh Refinement over Triangulated Surfaces, INRIA Res. Rep. No. 2462, June 1994.
[32] Arminjon, P. (1992). Two-dimensional finite volume extension of the Nessyahu-Tadmor scheme for conservation laws, private communication to A. Jameson, Princeton University, April 1992.